Published in: Journal of the European Ceramic Society (2021), vol. 41, n°1, pp. 669-683
DOI: 10.1016/j.jeurceramsoc.2020.07.046
Status : Postprint (Author's version)

Use of partial discharge patterns to assess the quality of sample/electrode contacts in flash sintering

J.-F. Fagnard[a,*], C. Gajdowski[b], L. Boilet[b], F. Henrotte[c], C. Geuzaine[c], B. Vertruyen[d], P. Vanderbemden[a]

[a] *Electronics, Microsystems, Measurements, and Instrumentation (EMMI), Department of Electrical Engineering and Computer Science Montefiore Institute, University of Liege, 4000 Liège, Belgium*

[b] *Belgian Ceramic Research Centre, avenue gouverneur Cornez, 4, 7000 Mons, Belgium*

[c] *Applied and Computational Electromagnetics (ACE), Department of Electrical Engineering and Computer Science Montefiore Institute, University of Liege, 4000 Liège, Belgium*

[d] *GREENMAT, CESAM Research Unit, University of Liege, 4000 Liège, Belgium*

KEYWORDS: Partial discharge; Flash sintering; Sample-electrode contact; In-situ monitoring technique

ABSTRACT

In a flash sintering process, a straightforward way to control the current uniformity through the sample is contacting the sample to the electrodes with platinum paste. This method is however costly for large-scale applications. We show that the in-situ phase resolved partial discharge technique is suitable to assess the quality of the contact between Pt electrodes and uncoated 3YSZ samples. In the temperature range 250-500 °C and for 50 Hz electric fields ramped up to 3.2 kV/cm, a sudden increase of the partial discharge current well before any curvature change of the 50 Hz current is found to be a signature of a defective electrical contact. Changes in the partial discharge amplitude are observed around the current rush. The surface microstructure of the samples subjected to partial discharges shows characteristics similar to those observed during dielectric breakdown, although the applied electric field is well below their typical dielectric strength.

1. Introduction

In the last decade, flash sintering (FS) has been successfully used to sinter a large number of materials of increasing complexity [1–18] at lower energetic cost [19–21]. Flash sintering experiments are usually carried out by regulating the voltage to a given value (stage I). For negative temperature coefficient materials, the resistance of the sample drops because of Joule heating and the current rises. At some point there is a current rush (stage II). In order to prevent an uncontrolled current rush, the current is stabilized at a pre-set limit value during a certain time (stage III). The sintering process occurs mostly in stage II and is continued at a slower rate during stage III where the grains grow [22]. The final densification is mainly ruled by the current density value. If the current density is too low, there is no optimal densification. However, if the current density is too high, there is a risk of current localization where overheating by the Joule effect can occur. This localization of current may result in generation of cracks and even the destruction of the sample. Other attempts to control the current have been studied like applying current ramps [23–25] or multiple steps [26].

A good current homogeneity is required for a successful flash sintering process. In general, studies are carried out on samples having a “dog bone” shape, with a reduced cross section middle part separating two “ears” drilled in order to place electrode wires. This geometry makes the current easy to control but it is not easy to implement for practical applications for the following reasons: (i) holes have to be drilled in the samples, and (ii) only a few mm^3 samples are obtained at the end. In view of sintering large volumes of material, planar platinum electrodes with large surfaces are needed. In this case, platinum paste is used as coating to improve the galvanic contact between the sample and the electrodes. For industrial applications, however, the use of platinum paste is not feasible because of its cost and the post-sintering machining required to remove it. It is nevertheless mandatory to achieve a homogeneous contact resistance without platinum paste in order to control the uniformity of the electrical current through the sample. This justifies the importance of an accurate characterization of the quality of the contact resistance between the platinum electrodes and the ceramic sample.

The goal of this work is to analyse the Partial Discharges (PDs) patterns obtained by the Phase Resolved Partial Discharge (PRPD) method as an in-situ measurement technique to assess the quality of the contact between the electrodes and the sample when no platinum paste is used.

Electrical Partial Discharges are defined [27] as “localized electrical discharges that only partially bridges the insulation between conductors and which can or cannot occur adjacent to a conductor. Partial discharges are in general a consequence of local electrical stress concentrations in the insulation or on the surface of the insulation. Generally, such discharges appear as pulses having a duration of much less than 1 μs”. Partial discharges are commonly separated in three groups depending on their origin. First, the Corona discharges are usually due to the local enhancement of

the electric field due to sharp points at the electrodes. Second, internal discharges originate from imperfections within the insulating material. Third, surface discharges occur at the surface of the insulating material where the tangential electric field is high. For several decades, partial discharge measurements have been routinely and extensively carried out to test and monitor the properties of insulating materials [28–33] or high-voltage equipment [34–36]. By contrast, there is very little work carried out on ceramic materials [37,38] at the notable exception of large permittivity piezoelectric materials such as $BaTiO_3$ or lead zirconate titanate [33,39,40]. In general, partial discharges in an insulating material cause various damages that can be detrimental on the long-term and may result ultimately in the dielectric breakdown.

In this paper we will consider the partial discharges on cylindrical 3 % yttria stabilised zirconia (YSZ) pre-sintered ceramic pellets of ~ 400 mm^3 placed between two platinum plates electrodes intended for flash sintering and will focus on the partial discharge patterns resulting from a possible imperfect contact with the Pt. The YSZ ceramics were subjected to an increasing AC electric field (f = 50 Hz) applied when the material was at a starting temperature between 250 °C and 500 °C. This temperature range was purposefully selected so that the partial discharge current brings relevant information.

2. Materials and methods

2.1. Sample preparation

Commercial tetragonal 3YSZ powders (TZ-3YSE, Tosoh USA, Grove City, OH, particle size of 90 nm) were uniaxially pressed in a cylindrical mould (inner diameter 12.5 mm). Samples were then pre-sintered to ~75 % relative density (see scanning electron micrographs in Fig. S1) during a 2 h dwell time in air at 1250 °C, in order to increase the mechanical resistance. Some of the pre-sintered pellets were then polished or machined into different geometries. The dimensions and shapes of all samples are presented in Fig. 1a and the corresponding photographs are shown in Fig. 1b. Samples A1 and A2 have flat unpolished surfaces. Samples from series B were polished with sandpaper to create flat (B1), rounded (B2, B3 and B4) or conical (B5) surfaces. Samples from series C were machined on one face to create one (sample C1) or four (sample C2) pyramidal tips with ~1 × 1 mm^2 basis and 0.5-0.6 mm height. The two faces of sample A2 were coated with platinum paste (Pt paste 5545, fired at 850 °C for 15 min).

2.2. Microscopic characterization

Scanning electron micrographs of sample C1 were collected in secondary electrons (SE) and back

scattering electrons (BSE) modes with a FEI XL30 ESEM combined with a QUANTAX Energy Dispersive X-Ray analysis system. The shaped and flat surfaces were coated with gold or carbon, respectively, to prevent charging.

Raman spectra were obtained with a Labram300 spectrometer interfaced using an Olympus BX40 microscope with a 532 nm diode laser, a short focal length Olympus x100 lens and a laser power of 4 mW on the sample.

2.3. ELECTRODES AND EXPERIMENTAL SETUP

Each YSZ sample was placed in a vertical tubular furnace between two planar Pt electrodes (25 mm x 25 mm x 1 mm) embedded in cylindrical blocks of grade 314 refractory stainless-steel (Fig. 2a and b). These blocks act as thermal mass to drain out heat produced within the sample during the application of the electric field. The edges of the blocks were rounded to limit the electric field concentrations when high voltage was applied. The Pt plate electrodes were connected to the secondary coil of the high voltage transformer with 1 mm diameter Pt wires (Fig. 2a), placed in alumina tubes for electrical insulation from the aluminium frame of the setup (Fig. 2c). The stainless-steel rods used to maintain the stainless-steel blocks were inserted in alumina tubes for the same reason (Fig. 2c). The lower rod was tied to the aluminium frame while the upper one was centred by a concentric alumina guide (Fig. 2c). The pressure applied to the sample/electrode contacts therefore resulted from the weight of the upper electrode + block + rod assembly.

Temperature was measured with two type K thermocouples. Thermocouple 1 was positioned in the furnace tube at the same height as the sample and was used to control the temperature of the furnace using a JUMO dTron 308 controller. Thermocouple 2 was anchored thermally to the back of the grounded upper Pt electrode through a hole in the stainless-steel block (Fig. 2c) and connected to a JUMO DICON touch controller. The signal from thermocouple 2 was found to be sensitive enough for determining whether self-heating occurred within the sample by comparison to the stable furnace temperature measured by thermocouple 1.

Figure 1. (a) Shapes and dimensions of the studied samples. The diameter of all samples ranges between 10.52 and 10.76 mm. The two faces of sample A2 were coated with platinum paste (thickness ~ 50-100 μm) and (b) Photographs of the studied samples.

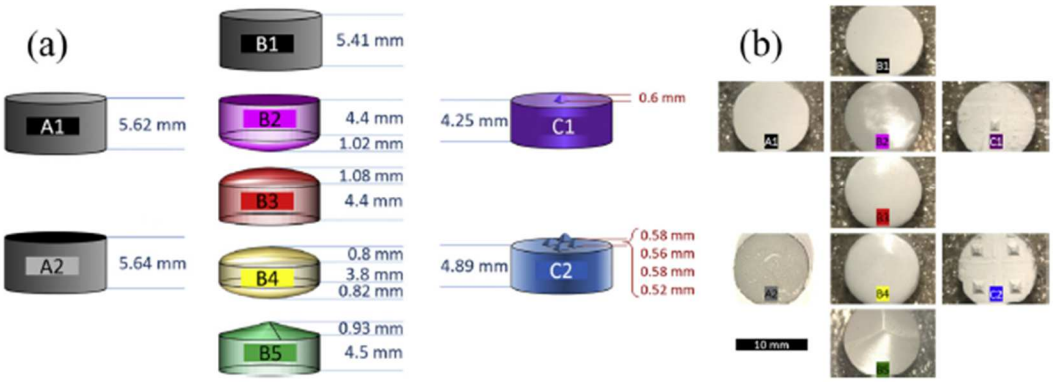

***Figure 2**. Experimental setup for the insertion of the sample inside the furnace: (a) Pt electrode in stainless-steel block; (b) sample sandwiched between electrodes; (c) general view with the aluminium frame moved to its highest position above the vertical tubular furnace to allow the sample placement. The hole in the stainless-steel block placed at the back upper Pt electrode is intended for the insertion of thermocouple 2, labelled T2.*

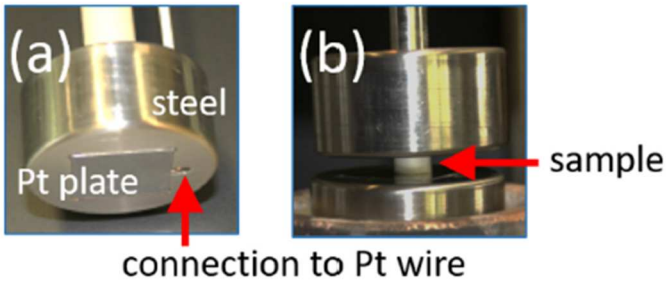

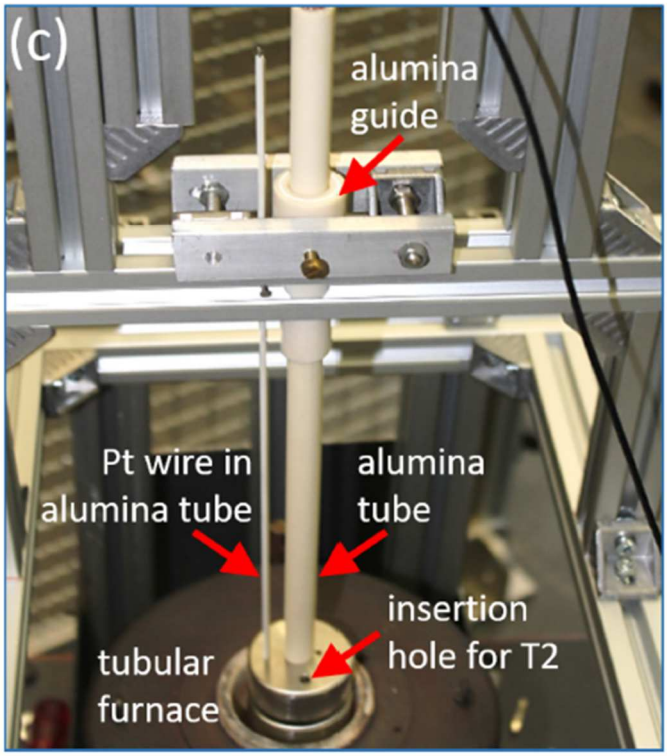

2.4. PARTIAL DISCHARGES DETECTION SYSTEM AND INSTRUMENTATION

Fig. 3a shows the experimental setup for the electrical measurements. A 50 Hz AC voltage (V) was applied to the sample through a high voltage transformer (1:240 ratio). In most experiments, the amplitude of V was increased in successive steps up to 1.8 kV (electric field E ~ 3.2 kV/cm, depending on the sample thickness). In other experiments, V was increased as a continuous ramp (25 V/s). For a better sensitivity, the current was not measured on the sample side of the transformer. Instead, the low frequency current (with its main component at 50 Hz) was measured in the primary winding with a current probe (Fluke i30 s) connected to a HP 34401A multimeter and a NI-USB-6366 data acquisition system and divided by 240 (transformation ratio) to obtain the current in the secondary winding (hereafter "current at 50 Hz, I_{50Hz}"). The voltage, electric field and current at 50 Hz are RMS values.

In order to measure partial discharges (PD), a specific measurement leg was connected in parallel to the main circuit (Fig. 3a). Since partial discharges are very short events, they appear as high frequency signals and a 1 nF coupling capacitor in series with a quadrupole was used to select the 40 kHz–800 kHz range. The amplitude (in coulombs) of each partial discharge was measured through a pre-amplifier and a main amplifier according to standards such as IEC60270 [27] by an Insulation Condition Monitoring (ICM) system from Power Diagnostix [41]. This measurement setup reverses the sign of the PD amplitude occurring in the sample/electrodes assembly. A dead time of 50 µs was applied to avoid multiple detections of the same PD due to the fading oscillating current in the measurement circuit. A Low-Level Detection (LLD) threshold of 4 pC was used to reject signals from ambient noise. The value of the LLD threshold was defined during preliminary experiments, based on the maximum discharge amplitude and the preamplifier and main amplifier gains.

Fig. 3b shows a typical “Phase Resolved Partial Discharges” (PRPD) pattern, plotting data collected during 60 s at a given applied AC voltage. Each measured partial discharge is a point in the pattern; the c olour code (from grey to red to orange to yellow in logarithmic progression) reflects the number of partial discharges with similar characteristics of amplitude (vertical axis) and time of occurrence with respect to the voltage sinewave period (20 ms period for a 50 Hz AC voltage). The horizontal axis is conventionally drawn as the phase of the applied voltage, from 0° to 360°, hence the name "phase-resolved" PD pattern.

The average discharge current I_{PD} is obtained from the PRPD pattern as the sum of the absolute amplitude values of all partial discharges divided by the total measurement time. I_{PD} is typically 5–6 orders of magnitude smaller than the current at 50 Hz.

2.5. NUMERICAL SIMULATIONS

Numerical simulations of the experimental setup were performed assuming, for the electrical conductivity of the YSZ samples, a simple homogeneous Arrhenius conductivity law. The parameters of this law were identified from electrical I(V) measurements carried out previously on pre-sintered 74 % dense samples with a shape similar to that sample A2; like for sample A2, Pt paste was used between the sample and the electrodes. The I(V) data were determined in a temperature range between 400 °C and 850 °C and under DC voltages between 0.1 V and 100 V applied using a Keithley 2400 voltage source. Currents up to 100 mA (limited by the source compliance) were measured using an Agilent 34401A multimeter. At low voltage (typically V < 20 V at T = 400 °C and V < 5 V at T = 850 °C), the I(V) curves exhibit a nearly ohmic behaviour following $V \sim I^n$ with n values between 0.96 and 1.31. The σ(T) data used in the modelling were always determined at an applied voltage V = 1V.

***Figure 3**. (a) Experimental setup for partial discharge detection and (b) Typical phase-resolved partial discharge pattern plot.*

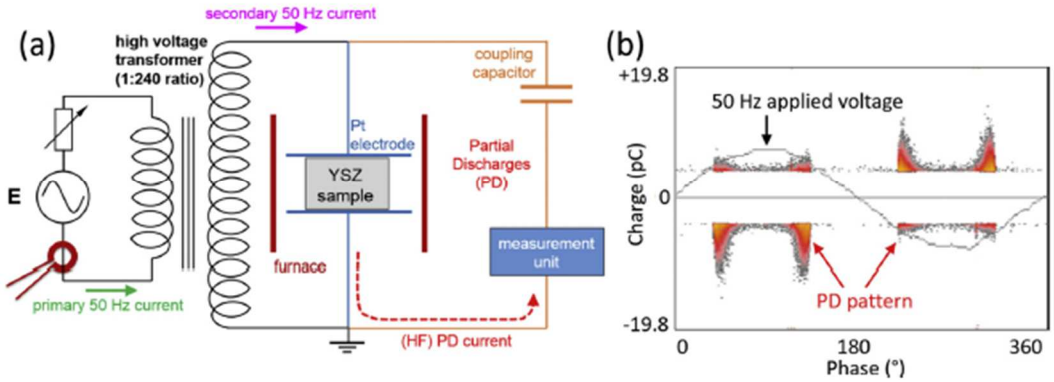

***Figure 4**. Current at 50 Hz (blue lines) and average discharge current I_{PD} (red lines) measured at 320 °C on YSZ pellet A1 with no Pt coating (plain lines) and on YSZ pellet A2 coated with Pt paste (dashed lines). E_{rush} is the electric field value for which the slope of the I_{50Hz}-E curve is ten times higher than in the ohmic regime below 1 kV/cm; $E_{inception}$ is the electric field for which IPD exceeds a threshold value just above the typical noise level of the experiment, here chosen to 0.6 nA (For interpretation of the references to colour in this figure legend, the reader is referred to the web version of this article).*

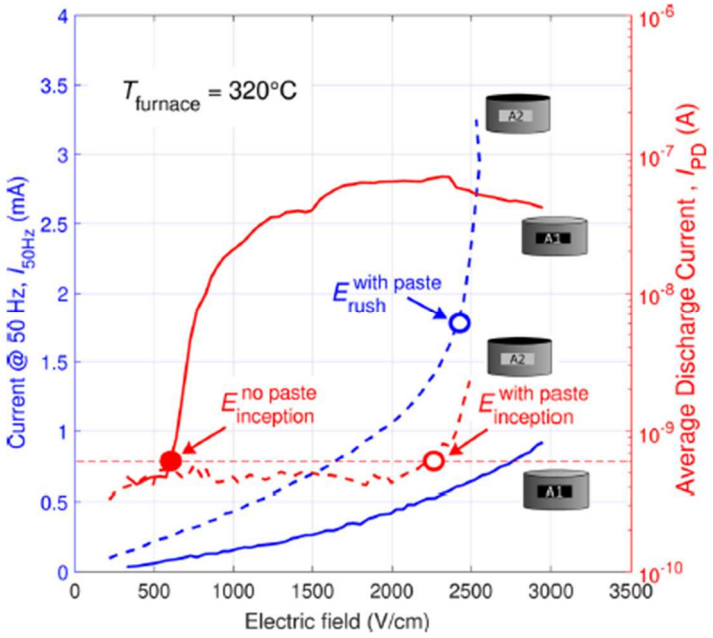

The developed multi-physical finite element model [42] allows to accurately reproduce the thermal conditions under which the sample is operated in the experimental set-up described above.

3. Results

Section 3.1 reports measurements of the current at 50 Hz and the average discharge current (defined in section 2.4) for YSZ pellets with/ without Pt paste coating, placed at different furnace temperatures or shaped with different geometries. Please note that in all graphs, the current at 50 Hz is plotted in linear scale while I_{PD} is much smaller and plotted in logarithmic scale. Section 3.2 focuses on a detailed analysis of the phase-resolved partial discharge patterns for samples with differentsample/electrodes contact areas. Section 3.3 examines the time evolution of partial discharges during experiments where the electric filed is increased as a ramp or in steps. Finally, Section 3.4 describes how the surface of the samples was affected by the partial discharge experiments.

3.1. INFLUENCE OF PT PASTE, FURNACE TEMPERATURE AND SHAPE OF PELLET SURFACES

The effect of a platinum paste coating on the sample-electrode contacts was investigated on samples A1 and A2. Both samples have flat surfaces, which were covered with Pt paste in the case of sample A2. Fig. 4 plots the current at 50 Hz (I_{50Hz}) and the average discharge current (IPD) as a function of the applied electric field, for a furnace temperature of 320 °C. The blue curves in Fig. 4 show that I_{50Hz} is two to three times lower for the uncoated sample than for the coated sample. For both samples, the slope of the $I_{50Hz\text{-}E}$ curve increases with the electric field. In the following, a "rush electric field" E_{rush} will be defined as the electric field value for which the slope of the $I_{50Hz\text{-}E}$ curve is ten times what it was in the ohmic regime below 1 kV/cm. For the Pt coated sample, E_{rush} is around 2.4 kV/cm, while for the sample without Pt coating, the slope is multiplied only by a factor of 2 at the highest electric field applied in our experiment, so that E_{rush} was not reached in the investigated range.

The occurrence of partial discharges is illustrated by the electric field dependence of the average discharge current IPD (red curves in Fig. 4). For both samples, the I_{PD}-E curve starts by a flat plateau which is followed by a marked increase. Hereafter, the "inception electric field" Einception is defined as the electric field for which IPD exceeds a threshold value taken just above the noise level of the experiment. In the present study, a 0.6 nA threshold value was found suitable for all YSZ samples investigated. For the Pt coated sample, $E_{inception}$ is 2.25 kV/cm. For the sample without Pt coating, Einception occurs at a much lower value (600 V/cm); the sharp increase of IPD by more than one order of magnitude is followed by a slower rise to values between 50 and 80 nA for E between 1.5 and 3 kV/cm. In view of investigating this behaviour, all experiments reported hereafter refer to YSZ pellets sandwiched between two platinum electrodes with no platinum paste.

Fig. 5 examines whether the behaviour observed previously for the uncoated sample is modified when the furnace temperature is stabilized at different temperatures (283 °C, 345 °C or 400 °C). The I_{50Hz} current (blue curves) increases with increasing temperature as expected from the positive temperature coefficient of the electrical conductivity. At 283 °C, I_{50Hz} is almost proportional to the electric field and the electric field corresponding to a current rush is not yet reached at the highest applied electric field (3.2 kV/cm). At higher temperatures, a strong deviation from Ohm's law can be observed with E_{rush} = 2.15 kV/cm at 345 °C and 1.5 kV/cm at 400 °C. Unlike E_{rush}, $E_{inception}$ (in the I_{PD}-E curves, in red) is almost temperature-independent and equal to ~600 V/cm. At 345 °C and 400 °C, a second rise in I_{PD} occurs in the vicinity of rush.

To gain further insight into the role of imperfect contact between the sample and the Pt electrodes, data were collected for uncoated pellets with flat (B1), rounded (B2, B3 and B4) or conical

(B5) surfaces. Average discharge current curves (not displayed here) show features similar to those reported previously: $E_{inception}$ in the range 600-700 V/ cm and I_{PD} in the range 1-100 nA between $E_{inception}$ and E_{rush}. Fig. 6 shows the I_{50Hz}-E curves at ~320 °C, revealing ohmic-like behaviour at small applied electric fields E < 1.5 kV/cm. This indicates that the reduced contact area at the electrode has little impact on the transport of current in this regime and suggests that self-heating effects are not significant. At higher electric fields, differences between the samples can be noticed, with progressively higher deviations from Ohm's law. Starting from sample B1 with two flat faces and no E_{rush}, the next sample is B2 with a rounded face at the grounded electrode and an E_{rush} of 2.95 kV/cm, just within the investigated range of electric fields. Finally, samples with a rounded (B3, B4) or conical (B5) surface in contact with the high-voltage electrode display E_{rush} in the 2.2–2.5 kV/cm range. The pellet with the conical surface (B5) exhibits the sharpest rise in I_{50Hz} above Erush.

3.2. INFLUENCE OF CONTACT AREA ON THE PHASE RESOLVED PARTIAL DISCHARGE PATTERNS

This section focuses on a more detailed analysis of the partial discharge behaviour using PRPD patterns, first in the case of sample B1 with flat surfaces and then on samples having one or several well-defined contact points. As detailed in the experimental section, each PRPD pattern plots partial discharges detected during a total measurement time of 60 s. The vertical axis corresponds to the amplitude (in pC) of the partial discharge and the horizontal axis shows the time of occurrence with respect to the voltage sinewave period, expressed as the phase of the applied voltage (from 0° to 360°). The colour code (from grey to yellow) reflects the number of partial discharges with similar characteristics.

***Figure 5**. Current at 50 Hz (blue lines) and average discharge current I_{PD} (red lines) measured on YSZ pellet B1 with no Pt coating at 283 °C, 345 °C and 400 °C. The values of E_{rush} are shown as solid symbols (For interpretation of the references to colour in this figure legend, the reader is referred to the web version of this article).*

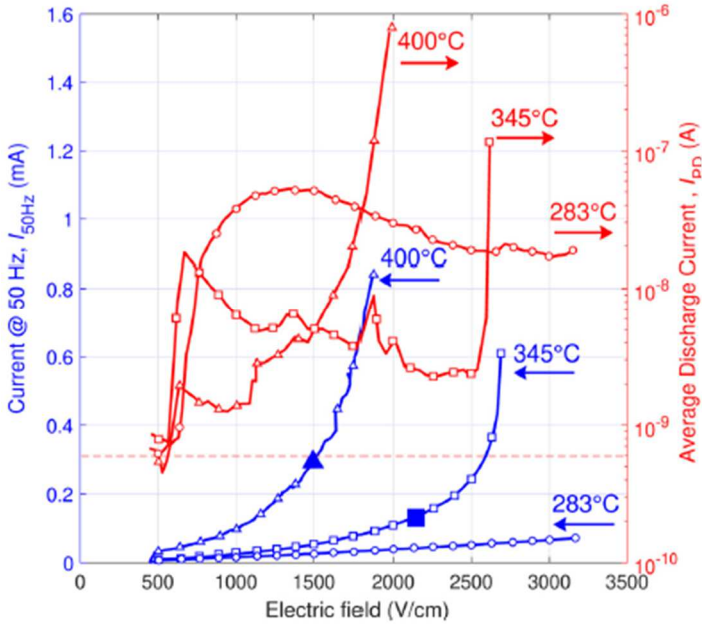

Figure 6. Current at 50 Hz measured on YSZ pellets with no Pt coating at 320 °C. HV = high voltage face; GND = grounded face; E_{rush} marked by solid symbol; see Fig. 1 for exact sample dimensions.

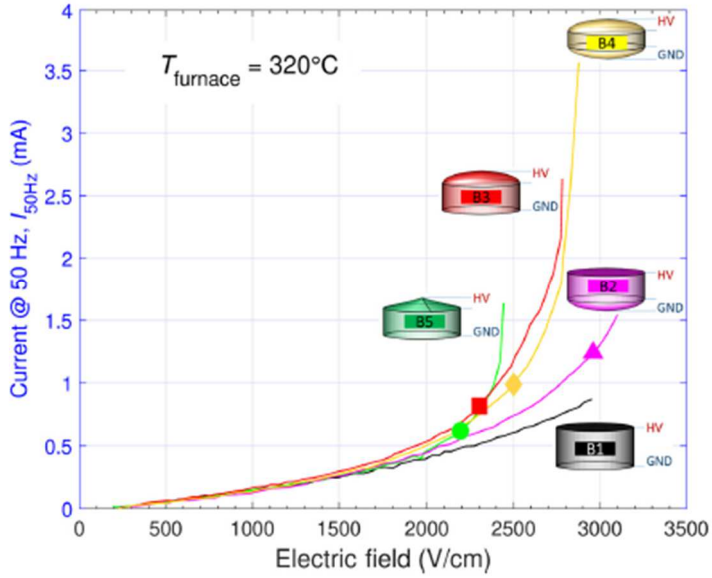

Fig. 7 shows PRPD patterns for the B1 pellet at 345 °C at 11 values of the applied electric field, labelled from A to K in the I_{PD} vs E curve. Below $E_{inception}$ (pattern A), there is no significant PD activity

except a few random discharges at the limit of the detection threshold. Above $E_{inception}$, I_{PD} rises to 20 nA with patterns B and C showing that the partial discharges occur when the instantaneous electric field is around its maximum value in the sinewave. The range of electric field in which PD occur is shown with green triangles in patterns B and C. In patterns D and E, partial discharges still occur in the same range of instantaneous electric field (800-1200 V/cm), so that the time of occurrence with respect to the period of the electric field sinewave moves away from the maximum electric field amplitude. Since the 800-1200 V/cm range is traversed faster than in patterns B or C, the partial discharge peaks become narrower (see also schematic in Fig. 7c) and the total PD intensity decreases down to 5 nA. The same sequence of events takes place several times in the I_{PD}-E curve (two of which are identified by the yellow diamond and magenta star symbols), with PD appearing in the range of maximum instantaneous field in patterns F and H (local maxima in the I_{PD}-E curve) and moving away as narrow peaks in patterns G and I. The final rise in I_{PD} (patterns J and K) starts again in the range of maximum instantaneous electric field (pattern J) and evolves into massive increase of partial discharges (pattern K) bringing the average discharge current above 100 nA beyond which the experiment was stopped. In summary, the examination of the PRPD patterns reveals that PD activity takes place when the instantaneous electric field is within well-defined intervals. The origin of the asymmetry in the PRPD patterns (between positive and negative charge as well as between positive and negative voltage half-cycle) is not clear but some of it can be attributed to the random character of PD occurrence over the 60 s collection time for each pattern.

The pellet B1 studied above is representative of the normal pellet geometry with flat surfaces. In order to investigate in a more controlled way the effect of the contact area, Fig. 8 shows typical examples of PRPD patterns collected at 345 °C on pellets C1 and C2 with respectively one and four pyramidal tips (see Fig. 1), where each tip exhibits an estimated area of about 0.25 mm^2 in contact with the high voltage electrode. In the case of sample C1, the PRPD patterns collected between $E_{inception}$ and Er_{ush} show that the PD activity is initiated in the range of maximum instantaneous electric field and then develops in a progressive manner instead of the successive waves observed for the sample B1 with flat surfaces. The PRPD patterns collected on sample C2 are much more complex: as suggested by arrows in Fig. 8b, it is possible to tentatively identify four bursts of partial discharges, which would match the number of pyramidal tips. These observations sustain the hypothesis that there is a connection between the occurrence of successive bursts of partial discharges and the presence of several localized contact points on the sample surface.

3.3. PARTIAL DISCHARGE ACTIVITY DURING A RAMP OR A STEP IN ELECTRIC FIELD

Sample C1 with one pyramidal tip in contact with the high voltage electrode is further

investigated in this section. Instead of focusing on the phase resolved patterns where the partial discharges are plotted as a function of their time of occurrence during the period of the voltage sinewave (20 ms), the graphs in this section follow the partial discharge activity over the 50 or 60 s of the experiment.

During the experiment depicted in Fig. 9, the sample temperature was stabilized at 345 °C (same temperature as previous section). Then the amplitude of the applied AC electric field was gradually increased (25 V/s) up to 3 kV/cm. Fig. 9 shows the time dependence of the electric field, the current at 50 Hz and the amplitude and number of partial discharges. The partial discharge activity increases first with the electric field up to a plateau and then suddenly decreases in the vicinity of E_{rush}. This decrease of the PD activity announces the runaway of the current at 50 Hz. When $I_{50\,Hz}$ reaches 1 mA, the extinction of the partial discharge activity is almost complete.

During the second set of experiments, the C1 sample was subjected to 15 steps of electric field between 1 kV/cm and 3.2 kV/cm, each of them applied for 55 s. The initial temperature of 385 °C was chosen to be higher than in the previous experiment so that E_{rush} is moved to a lower value. Fig. 10 plots the time evolution of the product of I_{50Hz} by the RMS voltage. This value expressed in VA corresponds to the average apparent power generated within the sample, regardless of its possible spatial distribution. The results plotted in Fig. 10 reveal three regimes, depicted as black, red and blue curves. For set values of electric field below 1.8 kV/cm (black curves), the power stays at a stable value below 0.4 VA. There is no evidence of a strong change of electrical conductivity due to a self-heating of the sample, suggesting that the power is effectively dissipated through the steel blocks in which the platinum electrodes are inserted. In this low electric field regime, the amplitude of partial discharges is an increasing function of the electric field but remains constant during each experiment (graphs A and B), except for the last black curve (set electric field of 1.8 kV/cm) where a decay of the partial discharge amplitude can be noticed over the duration of the experiment (graph C).

***Figure 7**. (a) Current at 50 Hz (blue line) and average discharge current I_{PD} (red line) measured on YSZ pellet B1 with no platinum coating at 345 °C. (b) Experimental Phase Resolved Partial Discharge patterns collected at several points in the I_{PD}-E curve, labelled from A to K. (c) Schematic illustration of the PD activity occurring in specific ranges of the electric field during the first half of the applied sinewave of the electric field; from top to bottom, the patterns illustrated are simplified representations of the three experimental patterns C, F and G (For interpretation of the references to colour in this figure legend, the reader is referred to the web version of this article).*

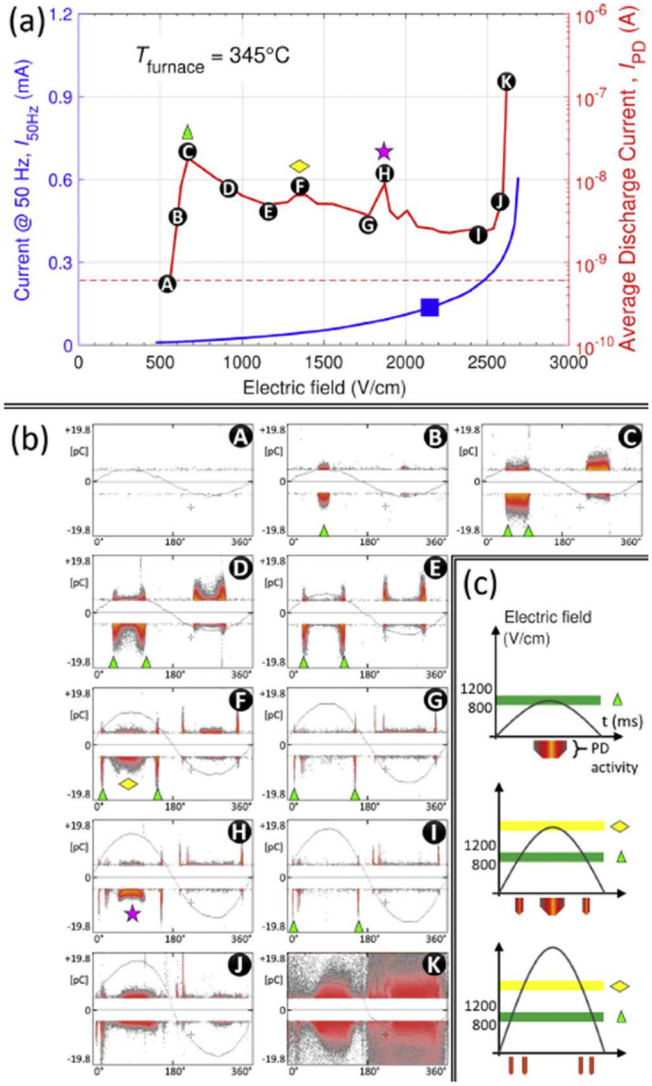

In the intermediate regime (red curves, set fields between 1.9 kV/cm and 2.1 kV/cm), the average power first appears to stabilize at values larger than 0.4 VA, but the thermocouple anchored through the steel block to the back of the upper Pt electrode reveals that the sample temperature starts to increase significantly. This temperature increase is thought to be due to the accumulated heat generated by the high current density at the sample tip. After an incubation period reminiscent of what is observed in flash sintering experiments, a jump in average power is observed, reflecting a

sudden increase of current due to a change of the sample impedance. As can be seen in graphs D, E and F, this jump is either preceded or followed by an almost complete disappearance of partial discharges. In the last regime (blue curve, set electric fields larger than 2.2 kV/cm), the self-heating of the sample accompanied by a decrease in the sample resistivity ρ is found to occur almost simultaneously with the increase in applied voltage. If the generator was purely voltage-regulated, the decrease of the sample resistivity would trigger the current rush. Due to the characteristics of the measurement setup, in the present case the average electric field across the sample falls back to a roughly constant value between 1.6 and 1.8 kV/cm, for which the power generated within the sample by the Joule effect (RI^2) balances the power drained out of the sample, mainly across the surface of the steel blocks (see Fig. 2a). In this regime the partial discharge activity is high and constant during the experiment (graph G.

Other experiments with steps in electric field were carried out for this sample C1 at furnace temperatures between 290 °C and 490 °C (not shown) and confirmed that the intermediate regime for this sample occurs within a narrow power range around 1 VA. The jump in power/ current always corresponded to a brutal change in the partial discharge activity, as was also observed in the vicinity of E_{rush} for the experiment with a ramp of electric field.

***Figure 8**. Phase Resolved Partial Discharge patterns for several values of the applied electric field between $E_{inception}$ and E_{rush}, collected at 345 °C on pellets (a) C1 and (b) C2 with no platinum coating. The last 2 patterns for sample C1 have a different range for the vertical axis.*

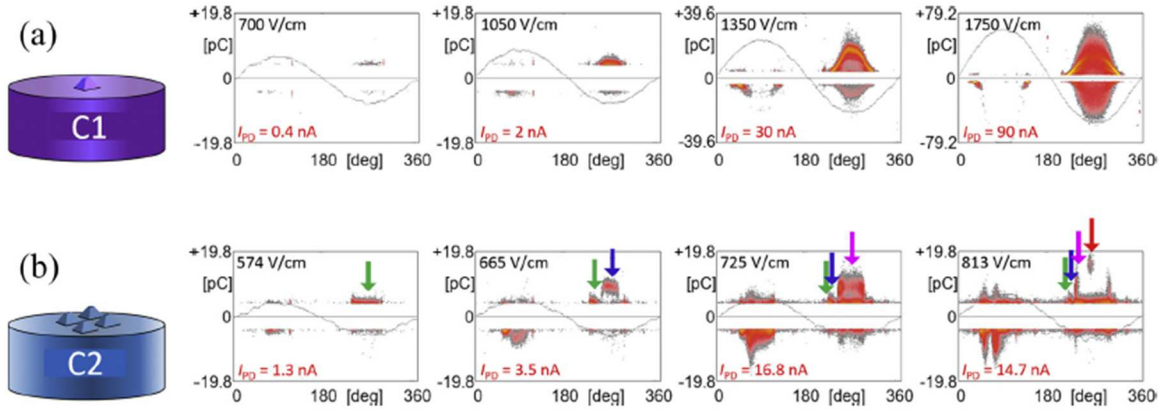

***Figure 9**. Partial discharges and current at 50 Hz for sample C1 at 345 °C during a ramp of electric field.*

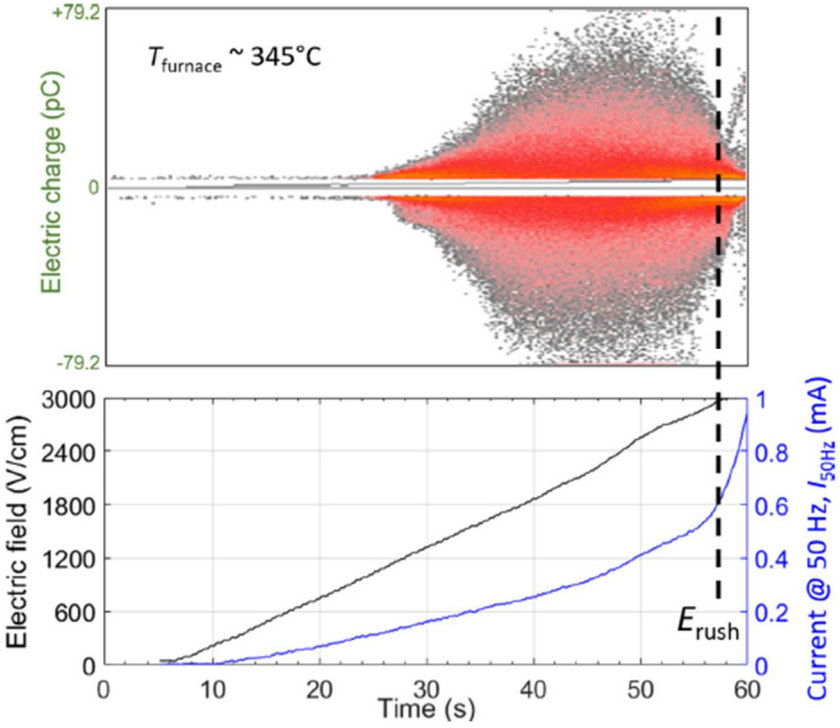

***Figure 10**. Main graph: Time evolution of the average power generated when sample C1 was subjected to steps of voltage corresponding to electric fields between 1 kV/ cm and 3.2 kV/cm, applied for 55 s at a furnace temperature of 385 °C. Small graphs: Time evolution of the partial discharge signal for set electric fields of (A) 1.3 kV/ cm, (B) 1.5 kV/cm, (C) 1.8 kV/cm, (D) 1.9 kV/cm, (E) 2 kV/cm, (F) 2.1 kV/cm and (G) 2.4 kV/cm. The dotted lines correspond to conditions where the measurement setup suppresses the current rush (see text).*

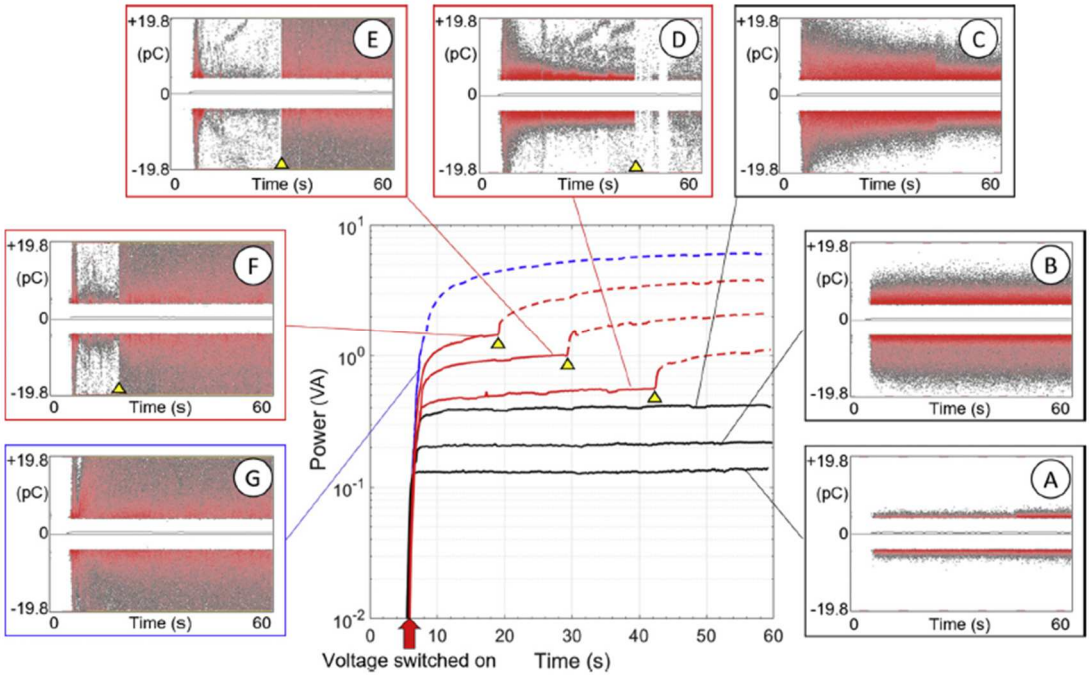

3.4. CHARACTERIZATION OF SAMPLE SURFACE AFTER PD EXPERIMENTS

Partial discharge experiments of moderate or high voltage amplitude often left visible marks on the sample surfaces, as shown by the optical micrographs collected in Fig. 11. These coloured traces appear as black or brown spots, irregular marks or halos on the initially white surface of the samples. They are usually localized at or around the areas of contact with the high voltage Pt electrode, but in the case of the sample C1, which was subjected to extensive PD experiments, they were also seen on the flat surface in contact with the low voltage Pt electrode. In the case of the smallest contact areas (sample B5, C1, C2), some of the marks can present metal-like shiny reflects. In the case of sample C2, the differences between the four pyramidal tips are probably due to the small difference in height between the four pyramids (not exceeding 60 µm).

Characterization of samples B3 and B5 by a combination of scanning electron microscopy coupled to Energy-Dispersive X-ray (SEM-EDX) analysis and Raman spectroscopy revealed that most of these marks correspond to platinum or carbon. All Back Scattered Electron micrographs in this paper are displayed with the usual scale of Z contrast so that platinum-coated areas appear whitish while carbon-rich zones appear in darker shades of grey than the zirconia matrix (Fig. 12). The presence of carbon residues was confirmed by Raman spectroscopy carried out in the black deposits compared to a pristine zone. The corresponding Raman spectra can be found in supplementary Fig. S2. The appearance of two broad Raman bands at 1350 cm^{-1} (D-band of sp^3 carbon) and 1580 cm^{-1} (G-band of sp^2 carbon) are characteristic of the presence of destructured carbon (mixture of sp^2 and sp^3 carbon).

Sample C1 (with one pyramidal tip) was characterized in particular detail since it had been subjected to an extensive range of partial discharge experiments.

Fig. 13a shows an overview of the central zone of the flat surface which was in contact with the low voltage electrode. BSE micrographs are presented in Fig. 13 to highlight compositional contrast but the corresponding SE micrographs are provided in Fig. S3. The numerous black spots in the optical micrograph appear here as nearly perfect circles (Fig. 13b) surrounded by a corona of platinum with a spray-like appearance (Fig. 13c). In many of them, platinum is also observed within the circle (Fig. 13d). The images in SE mode in Fig. S3 show that the circular area is depressed in comparison to the surrounding area. Most of the circular spots are found along polishing scratches, probably because the sharp edges of these scratches lead to an enhancement of the local electric field. Platinum deposits are occasionally observed along scratches (Fig. 13e), as already observed in

Fig. 12 for the rounded face of the B3 sample. Finally, the red rectangle in Fig. 13a singles out one of two unique features where the microstructure of the zirconia material is visibly altered (Fig. 13f, reproduced at higher magnification in Fig. S4) into swirling structures, interspersed with platinum areas. The similarity of these structures with the appearance of the pyramidal tip on the other face (see hereafter) suggests that this was probably a location of very intimate contact between the pellet and the platinum electrode.

As already observed in the sample with a conical surface (B5), the SEM/EDX characterization of the face of sample C1 in contact with the high voltage electrode revealed that only the pyramidal tip was affected by the PD experiments (Fig. 14). Platinum was found only at locations on the uppermost promontory, while the melted-like zirconia microstructure extended down to the next level.

4. Discussion

This discussion focuses on the main findings from the experiments reported above and evaluates how the insight brought by the partial discharge measurements relates to flash sintering experiments and to the dielectric breakdown of ceramics.

The experimental results on YSZ pellets without Pt coating show that $E_{inception}$ does not change significantly with temperature while E_{rush} moves to lower values when the temperature increases. In order to detect a low quality of electrode-sample contact by the sudden increase of the partial discharge current well before the current rush, the temperature should therefore be such that the condition $E_{inception} < E_{rush}(T)$ is met. This sets an upper bound for the temperature of the experiment. At the same time, in order to measure a 50 Hz current well above the noise level, the sample conductivity should be large enough, i.e. the temperature should be preferably higher than room temperature. The consequence is that a “medium” temperature range should be used. This medium temperature range depends on the sample size, geometry and electric properties and was found to be between 250 °C and 500 °C for the YSZ pellets investigated in the present study. In such conditions, the measurement of partial discharges can be used as an in-situ technique to assess the quality of the contact between metallic electrodes and the sample.

***Figure 11**. Optical micrographs of the surface of several pellets after PD experiments. The rectangles in various colours show the location of electron micrographs presented in later figures.*

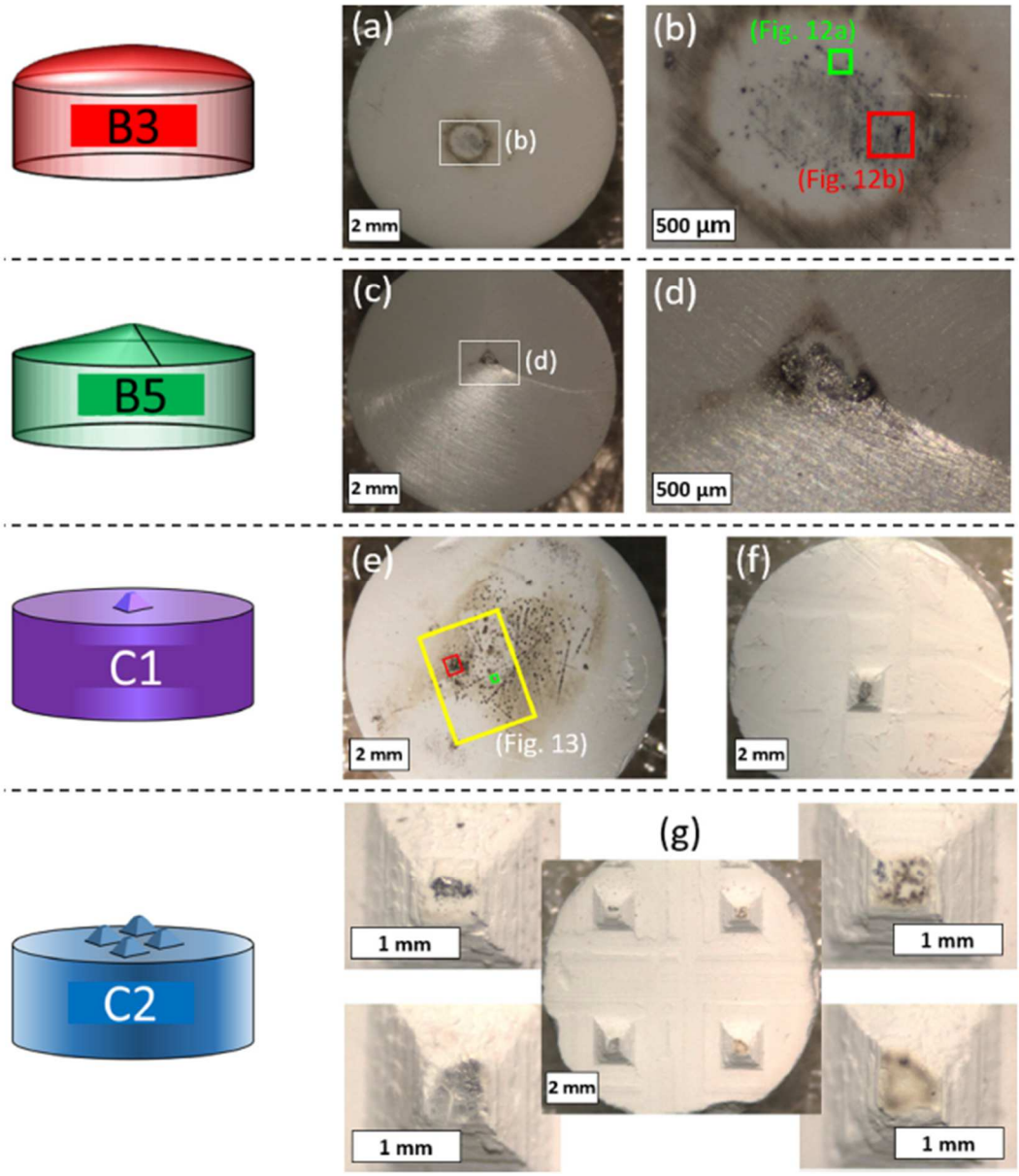

Based on these experiments, it is possible to build a picture of the partial discharge activity associated to the quality of sample/electrodes contacts. For all samples without Pt coating, the appearance of partial discharges at $E_{inception}$ occurs in the range 600-700 V/cm, well before any noticeable change of curvature in the I_{50Hz} vs. E curve. Coating the pellet with Pt paste (sample A2) increased the current at 50 Hz by a factor of 3 and suppressed almost completely the partial discharges below the threshold electric field corresponding to the current rush. This gives evidence that most partial discharges measured between Einception and Erush for uncoated samples are located at the sample- electrode interface and reflect a defective electrical contact when no Pt paste

is used. Since the bulk resistivity of the ceramic YSZ sample is still large (typically 10^6-10^9 Ωm) in the medium temperature range (250-500 °C) where the experiments are performed, it cannot be ruled out that some partial discharges may also occur in the bulk of the sample.

***Figure 12**. SEM micrographs of details appearing as black marks on the optical micrograph of the rounded surface of the B3 pellet (see Fig. 11 for location of these details). The small circular spot on the left micrograph was identified as carbon by EDX while the irregular shaped white trace in the right micrograph was identified as platinum.*

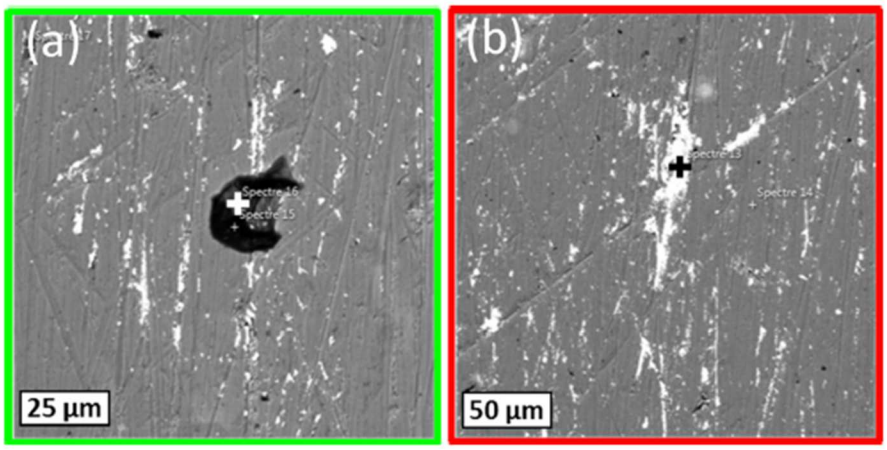

***Figure 13**. BSE micrographs of the flat surface of sample C1 (see Fig. 11 for the optical micrograph). Light grey areas were identified as platinum by EDX analysis.*

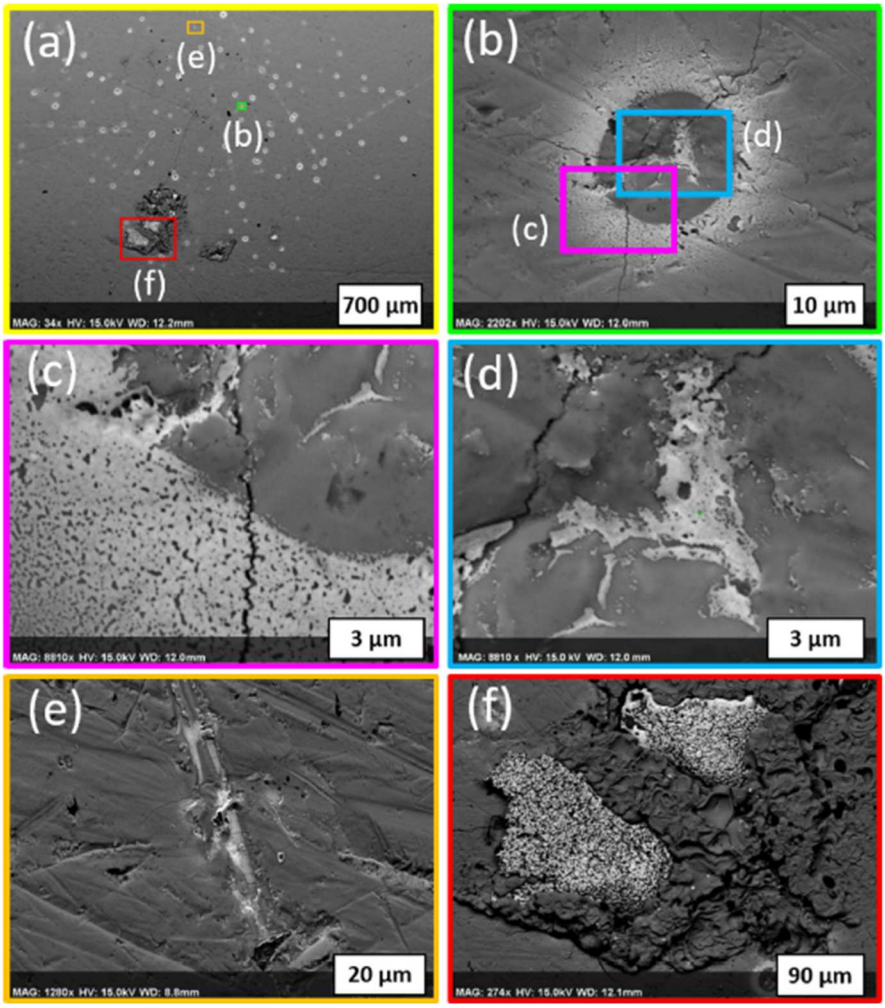

***Figure 14**. SE micrographs of the pyramidal tip of sample C1 (see Fig. 11 for the optical micrograph).*

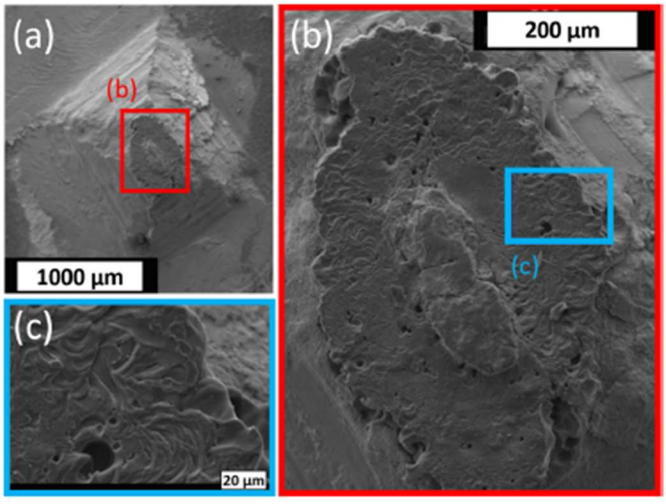

The experiments on the different series of pellets indicate that the $E_{inception}$ value does not change significantly with the shape of the sample surface, unlike E_{rush} which tends to decrease when the surface area in contact with the electrode decreases. Electric fields that are high enough (here exceeding 2 kV/cm) are needed to observe differences between the different shapes and hence to be sensitive to the reduced contact area. Comparison between samples B2 and B3 suggests that the effects of a reduced contact area are more pronounced for the electrode placed at high voltage than for the grounded electrode. In extreme cases where the sample-electrode contact is reduced to one or four pyramidal tips (samples C1 and C2), the appearance of successive bursts of partial discharges supports the hypothesis that their number could be associated to the number of local contact areas between the sample and the metallic electrodes. The transfer of platinum to the pellet surface (as a corona around circular spots, along polishing scratches, etc) and significant microstructure changes at the contact points were evidenced by the electronic microscopy and EDX results and suggest that the combination of a strong local electric field to a possibly elevated temperature gave rise to ejection of platinum from the electrode surface. It is important to consider that the average dissipated power during the experiments in the present study, i.e. the Joule losses averaged over the whole sample volume, are in the range of a few VA at most. However, the current density is much higher at the location of the localized contact with the electrode due to the reduced cross-section with respect to the grounded flat face. The ratio of cross-sections between both faces is approximately 10 in the case of sample B3 and 350 for sample C1. Therefore, the power per unit volume dissipated by Joule effect, given by ρJ^2, can locally be two to five orders of magnitude larger at the contact surface with the high voltage electrode than at the grounded electrode. In practice, however, this ratio of power density between faces is likely to be smaller than the estimation purely made of the ratio of cross-sections, since when a localized area heats up, its resistivity decreases. This indicates that the constriction of current resulting from an imperfect contact area between the YSZ sample and the electrode is a key element to be considered when no platinum paste is used.

Indeed, when compared to the samples having two flat surfaces (A1,A2,B1), the pellets exhibiting a smaller contact area actually display a higher current I_{50Hz} at high electric fields. This supports the picture in which the constricted current flow gives rise to a local self-heating. Since YSZ has a negative temperature coefficient for the electrical resistivity, self-heating drives the system towards a current rush, which takes place or not depending on the thermal boundary conditions. The temperature distribution results from the (un)balance between the heat produced within the sample by Joule effect and the heat drained out by conduction through the metallic electrodes, convection and radiation and therefore also function of the setup, sample geometries and thermal

properties. This is illustrated by the different regimes in Fig. 10, going from a balanced situation (black curves) to an incubation period preceding the current rush (red curves) to an immediate, self-heating-driven current rush (red curves).

Considering the thermal properties of the materials (sample and electrodes) and the boundary conditions of our set-up, numerical simulations provide a qualitatively good description of the thermal runaway phenomenon observed experimentally. Our experimental determination of the temperature dependence of the DC electrical conductivity on pre-sintered 74 % dense samples gives an activation energy of 1.03 eV. This value agrees well with activation energies reported in the literature, ranging between 0.92 and 1.7 eV [43–45]. The DC conductivity extrapolated at 283 °C agrees within 30 % with the AC conductivity (f = 50 Hz) calculated from the data of Fig. 5 at the same temperature and a 250 V applied voltage. The electrical conductivity measured in both DC and AC is found to increase with increasing amplitude of the applied voltage, as reported in other studies [46]. Quantitatively, the impedance of the sample modelled with this simple Arrhenius conductivity law appears to be underestimated by a factor between 6 and 10 depending on the situation, compared to available experimental data. Different explanations are possible to explain this underestimated impedance. As an example, the Maxwell-Wagner polarization phenomenon [47] confers zirconia samples a capacitive behaviour which explains therefore, in the harmonic regime (here at 50 Hz), an increased sample impedance. Numerical experiments have shown that accounting for this capacitive effect in the modelling does indeed increase the impedance of the sample, but also shifts the onset of the thermal runaway phenomenon up to electric field values significantly higher than those observed experimentally. Similarly, a homogeneous decrease of the bulk conductivity (by reducing the preexponential factor of the Arrhenius law) leads to the same result. A good matching of both the sample impedance and of the electric field at which the thermal runaway occurs can thus not be obtained with simulations that assume a homogeneous conductivity law. This leads us to conclude that it is indeed the effective cross-section of the current flow through the sample that must be somehow reduced. Another set of numerical experiments show that this hypothesis is indeed able to considerably improve the agreement between simulation and experiment and that a phenomenon of current localization in the sample necessarily comes into play. The analysis of the physico-chemical mechanisms allowing this current localization at the level of the microstructure of the material is however beyond the scope of this article. It is currently under investigation and will be presented in a further publication.

There is a strong demand in the flash sintering community to have exploitable data in order to improve the understanding of the mechanisms in play. In this study, the experiments were carried out at 50 Hz. However, the partial discharge measurement setup could advantageously be used at

other frequencies in order to investigate further the frequency dependence of both partial discharge patterns and the electrical conductivity at high electric fields. The conductivity data measured in such conditions could be compared to impedance spectroscopy measurements that are already used to distinguish the respective contributions of grain and grain boundaries [45]. In the DC regime, various polarity-induced effects have been reported: in zirconia such effects include blackening [48] or asymmetric grain growth [22]; in glasses they include asymmetric pore size [49]. In the AC regime, such polarity-induced effects are usually absent at moderate frequencies but some of them were recently observed at low frequency (~10 Hz and below) [50]. The simultaneous measurements of the current in phase with the applied voltage and the partial discharge patterns at very low frequency (< 1 Hz) could therefore provide useful information. As shown in our results, the bursts of partial discharge patterns are related to the presence of a finite number of localized areas presenting a strong sample-electrode contact. The pattern of partial discharges, therefore, could be put in relation with possible electrochemical reactions occurring at frequencies below 1 Hz.

It is interesting to note that the amplitude of the partial discharge signal is often found to change just before the rush in the current at 50 Hz. A noticeable decrease of the PD activity could be noticed just before E_{rush} when the voltage was applied as a ramp in Fig. 9. A complete modification of the PD activity was observed just before or after the current jump when the voltage was applied as a step in Fig. 10. Although these phenomena require much more investigation in order to be better understood, they suggest that the partial discharges amplitude might be an appropriate quantity to monitor the approach of the current rush, at least in the temperature range where the threshold electric field is larger than the inception electric field. Such an approach has been reported for systems detecting insulation deterioration, where a decrease in PD amplitude is used as a warning signal in order to prevent the current rush corresponding to the terminal failure of the insulation (dielectric breakdown) [34].

The similarities between flash sintering and dielectric breakdown were pointed out by Biesuz et al. [51] who observed the existence of an incubation time and chemical effects in alumina samples. Shi et al. [52] also made the link between dielectric breakdown and flash sintering in a work on donor-doped $BaTiO_3$; they notice the similarity of processes indicated by the current avalanche characteristics and explain it by the amplification of the local electric field strength at the particle contact because of the dielectric polarization of high permittivity particles. Recently, Liu et al. [53] have proposed that the flash sintering of a 99 % dense ZnO ceramic (achieved by applying a 3.53 kV/cm AC electric field during 40 s at room temperature) resulted from a partial dielectric breakdown initiated near the junction between silver paste and the cross-section shortening of their dog-bone sample followed by rapid expansion through the whole sample. They remark that in AC high-field

flash sintering, the geometry of the electrodes has a major impact on the sintering behaviour since sintering starts where the electric field is the highest. These findings can be put in parallel with the results of the present work, in which we showed that partial discharge activity is enhanced when no platinum paste is used, i.e. when the quality of the contact between the electrode and the ceramic sample is degraded.

It should be emphasized that $E_{inception}$ and E_{rush} values in the present study are much smaller than the dielectric breakdown field for the investigated YSZ material, which is typically of the order of 1.3 MV/cm [54]. However, the electric field enhancement at the sample-electrode interface in case of degraded contact (absence of platinum paste) probably mimics what happens at higher electric fields in the bulk of insulating ceramics, where partial discharges within the pores of the material are believed to initiate the dielectric breakdown. After the initiation stage, the ceramic may undergo a propagation stage and finally the ultimate breakdown stage which leads to the complete loss of the insulating properties of the material. In the following of this paragraph we provide a brief description of the dielectric breakdown phenomenon in a bulk insulator, based on literature references. During the initiation stage, because of the permittivity difference between the gas filling the pore and the bulk matrix, the electric field enhancement in the pores causes the gas breakdown and initiates partial discharges. The emitted electrons produce secondary electrons by interaction with the gas in the pores [55] and with the surface of the material [56]. This process depends on the nature of the gas, the permittivity and the resistivity of the material. It has been shown that materials having larger pores have lower partial discharge inception field and also lower breakdown field [33,57]. While the energy released by these individual partial discharges is rather small, under AC voltage the repeated production of electric charges over a long period of time would result in an increase of the local field and then in the temperature due to the Joule effect. The local temperature increase leads to temperature gradients which induce mechanical stress and the formation of microcracks. For larger field amplitude and exposure duration, the deterioration of the ceramic becomes more pronounced at/near the surface. Eventually the ceramics reaches the breakdown when a conductive channel opens through the sample associated to a big crater and irregularly arranged cracks at the surface as shown for alumina single crystals in [58]. The dissipated heat during or after the breakdown is so high that molten material is observed to enclose the breakdown channel and a certain amount of ceramic material is believed to vaporize during the breakdown event. The combined action of high electric fields and local self-heating gives thus rise to localized electric discharges, leading eventually to the dielectric breakdown [58].

Remarkably, the results in our study highlight that significant microstructural changes can occur at the location of point-like contacts between the electrodes and the sample, even though the

overall electric field is much below the field required for dielectric breakdown. The altered microstructure around the contact area and the contamination with platinum from the electrodes sustain the hypothesis that high temperatures are encountered in the zone where partial discharges are generated. Similar characteristics have been reported in the microstructures of flash-sintered ceramics like 8 %mol YSZ [59], BaTiO3 [60] or ZrO_2/Al_2O_3 composites [61]. In these samples, the constriction of the electric current was observed to lead to very high temperatures and strong modifications of microstructure. These observations confirm the strong correlation between dielectric breakdown/flash sintering and partial discharges even if the latter are less energetic.

5. Conclusion

In this paper, we analysed the electrical behaviour of cylindrical YSZ pellets subjected to AC electric fields up to ~ 3 kV/cm (50 Hz). The partial discharge patterns were measured by the Phase Resolved Partial Discharge (PRPD) method in experimental conditions similar to those used for flash sintering, except that the starting temperature before applying the electric field was lower than usual, here around 250-500 °C.

In this temperature range, a sudden increase of the partial discharge current well before any noticeable change of curvature of the 50 Hz current was found to be the signature of a defective electrical contact. Indeed, all YSZ pellets without Pt paste coating presented an inception electric field close to 600 V/cm, which appeared to be temperature independent. Between the inception electric field and the rush in the current at 50 Hz, various partial discharge patterns were found to develop, depending on the contact area with the Pt electrodes. Successive bursts of partial discharges might be related to the number of local contact areas between the sample and the metallic electrodes.

The partial discharge activity was also investigated in extreme cases where the sample-electrode contact was deliberately degraded by machining the pellet surface. Both Pt contamination and profound microstructure changes suggest that the local temperature might be very high due to the current localization. This confirms the importance of characterizing the quality of sample/electrode contact in order to avoid excessive current localizations in uncoated pellets during their sintering by flash process.

Declaration of Competing Interest

The authors declare that they have no known competing financial interests or personal relationships that could have appeared to influence the work reported in this paper.

Acknowledgement

This study is supported by ERDF and the Walloon Region, in the frame of IMAWA - FLASHSINT research project (program 2014–2020). The authors thank Dr C. Malherbe from ULiège for the Raman spectroscopy measurements. The authors thank M. Vedi Dupont from BCRC for the SEM observations.

Appendix A. Supplementary data

Supplementary material related to this article can be found, in the online version, at doi: https://doi.org/10.1016/j.jeurceramsoc.2020.07. 046.

References

[1] *M. Cologna, B. Rashkova, R. Raj, Flash sintering of nanograin zirconia in < 5 s at 850°C, J. Am. Ceram. Soc. 93 (2010) 3556–3559, https://doi.org/10.1111/j.1551- 2916.2010.04089.x.*

[2] *M. Cologna, A.L.G. Prette, R. Raj, Flash-sintering of cubic yttria-stabilized zirconia at 750°C for possible use in SOFC manufacturing, J. Am. Ceram. Soc. 94 (2011) 316–319, https://doi.org/10.1016/10.1111/j.1551-2916.2010.04267.x.*

[3] *A.L.G. Prette, M. Cologna, V. Sglavo, R. Raj, Flash-sintering of Co2MnO4 spinel for solid oxide fuel cell applications, J. Power Sources 196 (2011) 2061–2065, https:// doi.org/10.1016/j.jpowsour.2010.10.036.*

[4] *M. Cologna, J.S.C. Francis, R. Raj, Field assisted and flash sintering of alumina and its relationship to conductivity and MgO-doping, J. Eur. Ceram. Soc. 31 (2011) 2827–2837, https://doi.org/10.1016/j.jeurceramsoc.2011.07.004.*

[5] *E. Zapata-Solvas, S. Bonilla, P.R. Wilshaw, R.I. Todd, Preliminary investigation of flash sintering of SiC, J. Eur. Ceram. Soc. 33 (2013) 2811–2816, https://doi.org/10. 1016/j.jeurceramsoc.2013.04.023.*

[6] *H. Yoshida, Y. Sakka, T. Yamamoto, J.-M. Lebrun, R. Raj, Densification behaviour and microstructural development in undoped yttria prepared by flash-sintering, J. Eur. Ceram. Soc. 34 (2014) 991–1000, https://doi.org/10.1016/j.jeurceramsoc. 2013.10.031.*

[7] *R. Muccillo, E.N.S. Muccillo, Electric field-assisted flash sintering of tin dioxide, J. Eur. Ceram. Soc. 34 (2014) 915–923, https://doi.org/10.1016/j.jeurceramsoc. 2013.09.017.*

[8] *S.K. Jha, R. Raj, The effect of electric field on sintering and electrical conductivity of titania, J. Am. Ceram. Soc. 97 (2014) 527–534, https://doi.org/10.1111/jace. 12682.*

[9] *C. Schmerbauch, J. Gonzalez-Julian, R. Röder, C. Ronning, O. Guillon, Flash sintering of nanocrystalline zinc oxide and its influence on microstructure and defect formation, J. Am. Ceram. Soc. 97 (2014) 1728–1735, https://doi.org/10.1111/jace. 12972.*

[10] *A. Gaur, V.M. Sglavo, Densification of La0.6Sr0.4Co0.2Fe0.8O3 ceramic by flash sintering at temperature less than 100°C, J. Mater. Sci. 49 (2014) 6321–6332, https:// doi.org/10.1007/s10853-014-8357-2.*

[11] *L.A. Perez-Maqueda, E. Gil-Gonzalez, R. Raj, Flash sintering of highly insulating nanostructured phase-pure BiFeO3, J. Am. Ceram. Soc. 100 (2017) 3365–3369 https://doi.org/3365-3369, 10.1111/jace.14990.*

[12] *D. Kok, S.K. Jha, R. Raj, M.L. Mecartney, Flash sintering of a three -phase alumina, spinel, and yttria -stabilized zirconia composite, J. Am. Ceram. Soc. 100 (2017) 3262–3268, https://doi.org/10.1111/jace.14818.*

[13] *R. Chaim, G. Chevallier, A. Weibel, C. Estournès, Grain growth during spark plasma and flash sintering of ceramic nanoparticles: a review, J. Mater. Sci. 53 (2018) 3087, https://doi.org/10.1007/s10853-017-1761-7.*

[14] *X. Su, G. Bai, Y. Jia, Z. Wang, W. Wu, X. Yan, T. Ai, P. Zhao, L. Zhou, Flash sintering of lead zirconate titanate (PZT) ceramics: influence of electrical field and current limit on densification and grain growth, J. Eur. Ceram. Soc. 38 (2018) 3489–3497, https://doi.org/10.1016/j.jeurceramsoc.2018.04.007.*

[15] *M. Frasnelli, V.M. Sglavo, Flash sintering of tricalcium phosphate (TCP) bioceramics, J. Eur. Ceram. Soc. 38 (2018) 279–285, https://doi.org/10.1016/j. jeurceramsoc.2017.08.004.*

[16] *L. Spiridigliozzi, L. Pinter, M. Biesuz, G. Dell'Agli, G. Accardo, M.V. Sglavo, Gd/Sm- Pr Co-doped Ceria: a first report of the precipitation method effect on flash sintering, Materials 12 (2019) 1218, https://doi.org/10.3390/ma12081218.*

[17] *E. Taghaddos, H. Charalambous, T. Tsakalakos, A. Safari, Electromechanical properties of flash sintered BNT-based piezoelectric ceramic, J. Eur. Ceram. Soc. 39 (2019) 2882–2888, https://doi.org/10.1016/j.jeurceramsoc.2019.03.050.*

[18] *M. Soleimany, M.H. Paydar, Investigation on flash sintering of BaZr0.1Ce0.7Y0.2O3-δ compound; using nickel wire as electrode material, Ceram. Int. 46 (2020) 2128–2138, https://doi.org/10.1016/j.ceramint.2019.09.196.*

[19] *D. Sohrabi, B. Heidary, M. Lanagan, C.A. Randall, Contrasting energy efficiency in various ceramic sintering processes, J. Eur. Ceram. Soc. 38 (2018) 1018–1029, https://doi.org/10.1016/j.jeurceramsoc.2017.10.015.*

[20] *T. Ibn-Mohammed, C.A. Randall, K.B. Mustapha, J. Guo, J. Walker, S. Berbano, S.C.L. Koh, D. Wang, D.C. Sinclair, I.M. Reaney, Decarbonising ceramic manufacturing: a techno-economic analysis of energy efficient sintering technologies in the functional materials sector, J. Eur. Ceram. Soc. 39 (2019) 5213–5235, https:// doi.org/10.1016/j.jeurceramsoc.2019.08.011.*

[21] *M. Biesuz, V.M. Sglavo, Flash sintering of ceramics, J. Eur. Ceram. Soc. 39 (2019) 115–143, https://doi.org/10.1016/j.jeurceramsoc.2018.08.048.*

[22] *K. Ren, J. Xia, Y. Wang, Grain growth kinetics of 3 mol. % yttria-stabilized zirconia during flash sintering, J. Eur. Ceram. Soc. 39 (2019) 1366–1373, https://doi.org/ 10.1016/j.jeurceramsoc.2018.11.032.*

[23] *H. Charalambous, S.K. Jha, K.H. Christian, R.T. Lay, T. Tsalalakos, Flash sintering using controlled ramp, J. Eur. Ceram. Soc. 38 (2018) 3689–3693, https://doi.org/ 10.1016/j.jeurceramsoc.2018.04.003.*

[24] *M.K. Kumar, D. Yadav, J.-M. Lebrun, R. Raj, Flash sintering with current rate: a different approach, J. Am. Ceram. Soc. 102 (2019) 823–835, https://doi.org/10. 1111/jace.16037.*

[25] *K.H. Christian, H. Charalambous, S.K. Jha, T. Tsakalakos, Current-ramp assisted sintering of 3YSZ: electrochemical and microstructural comparison to flash and thermal sintering, J. Eur. Ceram. Soc. 40 (2019) 436–443, https://doi.org/10. 1016/j.jeurceramsoc.2019.09.036.*

[26] *J.V. Campos, I.R. Lavagnini, R.V. de Sousa, J.A. Ferreira, E.M. de Jesus Agnolon Pallone, Development of an instrumented and automated flash sintering setup for enhanced process monitoring and parameter control, J. Eur. Ceram. Soc. 39 (2019) 531–538, https://doi.org/10.1016/j.jeurceramsoc.2018.09.002.*

[27] *IEC 60270, High Voltage Test Techniques. Partial Discharge Measurements, (2015).*

[28] *S.M. Korobeynikov, A.G. Ovsyannikov, A.V. Ridel, D.I. Karpov, Study of partial discharges in bubbles and microsphere in transformer oil, J. Phys. Conf. Ser. 1128 (2018) 012118, https://doi.org/10.1088/1742-6596/1128/1/012118.*

[29] *J.M. Wetzer, Detecting voids in glass-bead devices with partial discharges induced by external fields, IEEE 1997 Annual Report Conference on Electrical Insulation and Dielectric Phenomena 2 (1997) 521–524, https://doi.org/10.1109/CEIDP.1997. 641125.*

[30] *T. Hori, N. Yanaze, M. Kozako, M. Hikita, J. Wada, S. Okabe, Partial discharge characteristics of epoxy composite with micro-meter size hollow glass particles, IEEE Conference on Electrical Insulation and*

Dielectric Phenomena (2015) 366–369, https://doi.org/10.1109/CEIDP.2015.7352113.

[31] *M. Kannan, P. Sreejaya, Partial discharge detection in solid dielectrics, Int. J. Sci. Eng. Res. 4 (2013) 1–6.*

[32] *K. Theodosiou, D. Agoris, I. Gialas, I. Vitellas, Measurements of partial discharges and power losses in pet films in high voltage AC fields, J. Electr. Eng. 58 (2007) 250–256.*

[33] *B.-C. Shin, S.-C. Kim, C.-W. Nahm, S.-J. Jang, Nondestructive testing of ceramic capacitors by partial discharge method, Mater. Lett. 50 (2001) 82–86, https://doi. org/10.1016/S0167-577X(00)00420-1.*

[34] *G.J. Paoletti, A. Golubev, Partial discharge theory and technologies related to medium-voltage electrical equipment, IEEE Trans. Ind. Appl. 37 (2001) 90–103, https://doi.org/10.1109/28.903131.*

[35] *C. Kane, A. Golubev, Advantages of continuous monitoring of partial discharges in rotating equipment and switchgear, Conference Record of the 2003 Annual Pulp and Paper Industry Technical Conference (2003) 117–122 https://doi.org/ 10.1109/PAPCON.2003.1216907.*

[36] *R. Nikjoo, N. Taylor, H. Edin, Effect of high voltage impulses on partial discharge characteristics of oil-impregnated paper for online diagnostics, IEEE International Power Modulator and High Voltage Conference (2016) 151–156, https://doi.org/ 10.1109/IPMHVC.2016.8012807.*

[37] *C.F. Bayer, U. Waltrich, A. Soueidan, E. Baer, A. Schletz, Partial discharges in ceramic substrates - correlation of electric field strength simulations with phase resolved partial discharge measurements, International Conference on Electronics*
Packaging (2016) 530–535, https://doi.org/10.1109/ICEP.2016.7486884.

[38] *T.A.T. Vu, J. Augé, O. Lesaint, M.T. Do, Partial discharges in aluminium nitrite ceramic substrates, 10th IEEE International Conference on Solid Dielectrics (2010) 1–4, https://doi.org/10.1109/ICSD.2010.5568137.*

[39] *T. Hang, J. Glaum, T. Phung, M. Hoffman, Investigation of partial discharge and fracture strength in piezoelectric ceramics, J. Am. Ceram. Soc. 97 (2014) 1905–1911, https://doi.org/10.1111/jace.12875.*

[40] *T. Hang, J. Glaum, Y.A. Genenko, T. Phung, M. Hoffman, Investigation of partial discharge in piezoelectric ceramics, Acta Mater. 102 (2016) 284–291, https://doi. org/10.1016/j.actamat.2015.09.031.*

[41] *https://pdix.com/.*

[42] *P. Dular, C. Geuzaine, F. Henrotte, W. Legros, A general environment for the treatment of discrete problems and its application to the finite element method, IEEE Trans. Magn. 34 (1998) 3395–3398, https://doi.org/10.1109/20.717799.*

[43] *R. Ramamoorthy, D. Sundararaman, S. Ramasamy, Ionic conductivity studies of ultrafine-grained yttria stabilized zirconia polymorphs, Solid State Ion. 123 (1999) 271–278, https://doi.org/10.1016/S0167-2738(99)00103-4.*

[44] *R.I. Todd, E. Zapata-Solvas, R.S. Bonilla, T. Sneddon, P.R. Wilshaw, Electrical characteristics of flash sintering: thermal runaway of Joule heating, J. Eur. Ceram. Soc. 35 (2015) 1865–1877, https://doi.org/10.1016/j.jeurceramsoc.2014.12.022.*

[45] *S.P.S. Badwal, Grain boundary resistivity in zirconia-based materials: effect of sintering temperatures and impurities, Solid State Ionic s 76 (1995) 67–80, https:// doi.org/10.1016/0167-2738(94)00236-L.*

[46] *C. Neusel, H. Jelitto, G.A. Schneider, Electrical conduction mechanism in bulk ceramic insulators at high*

voltages until dielectric breakdown, J. Appl. Phys. 117 (2015) 154902, https://doi.org/10.1063/1.4917208.

[47] *T. Prodromakis, C. Papavassiliou, Engineering the Maxwell-Wagner polarization effect, Appl. Surf. Sci. 255 (2009) 6989–6994, https://doi.org/10.1016/j.apsusc. 2009.03.030.*

[48] *J. Janek, C. Korte, Electrochemical blackening of yttria-stabilized zirconia – morphological instability of the moving reaction front, Solid State Ion. 116 (1999) 181–195, https://doi.org/10.1016/S0167-2738(98)00415-9.*

[49] *M.O. Prado, M. Biesuz, M. Frasnelli, F.E. Benedetto, V.M. Sglavo, Viscous flow flash sintering of porous silica glass, J. Non. Solids 476 (2017) 60–66, https://doi.org/10. 1016/j.jnoncrysol.2017.09.024.*

[50] *M. Biesuz, L. Pinter, T. Saunders, M. Reece, J. Binner, V.M. Sglavo, S. Grasso, Investigation of electrochemical, optical and thermal effects during flash sintering of 8YSZ, Materials 11 (2018) 1214–1228, https://doi.org/10.3390/ma11071214.*

[51] *M. Biesuz, P. Luchi, A. Quaranta, V.M. Sglavo, Theoretical and phenomenological analogies between flash sintering and dielectric breakdown in α-alumina, J. Appl. Phys. 120 (2016) 145107, https://doi.org/10.1063/1.4964811.*

[52] *R. Shi, Y. Pu, J. Ji, J. Li, X. Guo, W. Wang, M. Yang, Correlation between flash sintering and dielectric breakdown behavior in donor-doped barium titanate ceramics, Ceram. Int. 46 (2020) 12846–12851, https://doi.org/10.1016/j.ceramint. 2020.02.055.*

[53] *J. Liu, X. Li, X. Wang, R. Huang, Z. Jia, Alternating current field flash sintering 99% relative density ZnO ceramics at room temperature, Scr. Mater. 176 (2020) 28–31, https://doi.org/10.1016/s.scriptamat.2019.09.026.*

[54] *O. Jongprateep, V. Petrovsky, F. Dogan, Effects of yttria concentration and microstructure on electric breakdown of yttria stabilized zirconia, J. Metals Mater. Miner. 18 (2008) 9–14.*

[55] *I.O. Owate, R. Freer, Ac breakdown characteristics of ceramic materials, J. Appl. Phys. 72 (1992) 2418–2422, https://doi.org/10.1063/1.351586.*

[56] *T.B. Holland, U. Anselmi-Tamburini, D.V. Quach, T.B. Tran, A.K. Mukherjee, Local field strengths during early stage field assisted sintering (FAST) of dielectric materials, J. Eur. Ceram. Soc. 32 (2012) 3659–3666, https://doi.org/10.1016/j. jeurceramsoc.2012.03.012.*

[57] *V. Fuertes, M.J. Cabrera, J. Seores, D. Muñoz, J.F. Fernández, E. Enríquez, Microstructural study of dielectric breakdown in glass-ceramics insulators, J. Eur. Ceram. Soc. 39 (2019) 376–383, https://doi.org/10.1016/j.jeurceramsoc.2018.08. 044.*

[58] *C. Neusel, H. Jelitto, D. Schmidt, R. Janssen, F. Felten, G.A. Schneider, Dielectric breakdown of alumina single crystals, J. Eur. Ceram. Soc. 32 (2012) 1053–1057, https://doi.org/10.1016/j.jeurceramsoc.2011.11.013.*

[59] *M.C. Steil, D. Marinha, Y. Aman, J.R.C. Gomes, M. Kleitz, From conventional ac flash-sintering of YSZ to hyper-flash and double flash, J. Eur. Ceram. Soc. 33 (2013) 2093–2101, https://doi.org/10.1016/j.jeurceramsoc.2013.03.019.*

[60] *H. Yoshida, A. Uehashi, T. Tokunaga, K. Sasaki, T. Yamamoto, Formation of grain boundary second phase in BaTiO3 polycrystal under a high DC electric field at elevated temperatures, J. Ceram. Soc. Jpn. 124 (2016) 388–392, https://doi.org/ 10.2109/jcersj2.15259.*

[61] *C.L. Ojaimi, J.A. Ferreira, A.L. Chinelatto, A.S.A. Chinelatto, E.M. de Jesus Agnolon Pallone, Microstructural analysis of ZrO2/Al2O3 composite: flash and conventional sintering, Ceram. Int. 46 (2020) 2473–2480, https://doi.org/10.1016/j.ceramint. 2019.09.241.*